Journal of Solid State Chemistry 184 (2011) 2756–2761

Contents lists available at SciVerse ScienceDirect

Journal of Solid State Chemistry

journal homepage: www.elsevier.com/locate/jssc

Synthesis, structure and magnetism of a *S*-shaped multi-iron substituted arsenotungstate containing a trivacant Keggin $[B\text{-}\alpha\text{-}As^{V}W_9O_{34}]^{9-}$ and a hexavacant Keggin $[\alpha\text{-}As^{V}W_6O_{26}]^{11-}$ fragments

Junwei Zhao [a,*], Qiuxia Han [a,b], Dongying Shi [a], Lijuan Chen [a,b], Pengtao Ma [a], Jingping Wang [a], Jingyang Niu [a,*]

[a] Institute of Molecular and Crystal Engineering, College of Chemistry and Chemical Engineering, Henan University, Kaifeng, Henan 475004, PR China
[b] Basic Experiment Teaching Center, Henan University, Kaifeng, Henan 475004, PR China

ARTICLE INFO

Article history:
Received 17 May 2011
Received in revised form
1 August 2011
Accepted 14 August 2011
Available online 23 August 2011

Keywords:
Polyoxometalate
Arsenotungstate
Iron
Asymmetrical sandwich-type structure

ABSTRACT

A *S*-shaped multi-iron substituted arsenotungstate $[enH_2]_2[(\alpha\text{-}H_2As^{V}W_6O_{26})Fe_3(H_2O)(B\text{-}\alpha\text{-}H_4As^{V}W_9O_{34})]_2[Fe]_2\cdot 8H_2O$ (**1**) (en=ethylenediamine) has been prepared by reaction of $K_{14}[As^{III}_2W_{19}O_{67}(H_2O)]\cdot nH_2O$ with $Fe_2(SO_4)_3\cdot xH_2O$ under hydrothermal conditions and structurally characterized by elemental analyses, IR spectra, UV spectra, powder X-ray diffraction (PXRD) and single-crystal X-ray diffraction. The skeleton of **1** consists of two asymmetric sandwich-type subunits $[(\alpha\text{-}H_2As^{V}W_6O_{26})Fe_3(H_2O)(B\text{-}\alpha\text{-}H_4As^{V}W_9O_{34})]^{5-}$ linked by a di-Fe^{III} cluster. Moreover, magnetic susceptibility measurements demonstrate that **1** indicates the antiferromagnetic coupling interactions within Fe^{III} centers with the best-fitting set of parameters of $J_1=-7.07\ cm^{-1}$, $J_2=-0.45\ cm^{-1}$ and $g=2.05$, which are generated by the addition of the expressions of the molar susceptibilities of two tri-Fe^{III} clusters and one di-Fe^{III} cluster derived from for spin pairs coupled through the isotropic exchange interactions.

1. Introduction

Currently, the precursor approach to the design and synthesis of high-nuclear aggregates is a major focus of research. As we know, polyoxometalates (POMs), as a rapidly growing class of metal–oxygen clusters with versatile structural topologies, oxygen-enriched surfaces and interesting properties [1–7], are one of the excellent candidates for preparing novel larger aggregates. Among them, the divacant tungstoarsenate(III) $[As^{III}_2W_{19}O_{67}(H_2O)]^{14-}$ (abbreviated as $As^{III}_2W_{19}$) derived from the parent $[As^{III}_2W_{21}O_{69}(H_2O)]^{6-}$ polyoxoanion is constructed from two trivacant Keggin $[\alpha\text{-}As^{III}W_9O_{33}]^{9-}$ moieties linked by a WO_6 octahedron and can be used as the potential precursor to bond transition-metal (TM), lanthanide (Ln) and organometal (OM) cations. In comparison with the trivacant $[\alpha\text{-}As^{III}W_9O_{33}]^{9-}$ precursor, to date, only a few investigations on the reactions of $As^{III}_2W_{19}$ with TM, Ln and OM cations have been made although $As^{III}_2W_{19}$ was firstly discovered in 1973 [8]. For example, in 1975, Tourné et al. [9] studied the interactions of $As^{III}_2W_{19}$ with Zn^{II}, Co^{II} and Mn^{II} cations, leading to $[As^{III}_2W_{19}M_2O_{67}(H_2O)_2]^{10-}$ (M=Zn^{II}, Co^{II}, Mn^{II}). In 2001, Kortz et al. [10] determined the solid-state structure of $As^{III}_2W_{19}$ and used it as the precursor to prepare the large aggregate $[As^{III}_6W_{65}O_{217}(H_2O)_7]^{26-}$. Later, Kortz et al. again facilitated $As^{III}_2W_{19}$ to interact with $Sn(CH_3)_2Cl_2$ and $TiOSO_4$, respectively, forming $[\{Sn(CH_3)_2(H_2O)_2\}_3(\beta\text{-}As^{III}W_9O_{33})]^{3-}$ and $[Ti_2(OH)_2As^{III}_2W_{19}O_{67}(H_2O)]^{8-}$ [11,12]. Based on $As^{III}_2W_{19}$, Wang et al. synthesized a dimeric 3*d*–4*f* heterometallic POM $La[As^{III}_2W_{20}CuO_{67}(H_2O)_3]^{3-}$ and a novel aggregate $[As^{III}_4W_{19}O_{69}]^{12-}$ [13,14]. In 2009, a gadolinium-bridged POM nanocluster $[Gd_8As^{III}_{12}W_{124}O_{432}(H_2O)_{22}]^{60-}$ was thus obtained by Hussain et al. [15]. Obviously, the reported reactions containing the $As^{III}_2W_{19}$ precursors were mostly performed at atmospheric pressure and temperatures below 100 °C, however, the hydrothermal reactions of $As^{III}_2W_{19}$ with TM cations in the participation of organic components remain less explored. With the aim of discovering novel TM substituted arsenotungstates, recently, we have launched our exploration on the hydrothermal behavior of $As^{III}_2W_{19}$ based on the following reasons: (a) the structural diversity and facile polymerization of arsenotungstates are thus likely to result in the formation of unique large aggregates with unexpected structures and properties; (b) $As^{III}_2W_{19}$ has a versatile isomerization behavior in an aqueous solution and can transform to multiple types of its derivative units; and (c) hydrothermal environments can make a reaction shift from the thermodynamic direction to the kinetic so that its *in-situ* derivative units can promptly combine with TM cations to provide a precondition for creating novel TM substituted phases. Herein we report the synthesis, structural characterization and magnetic properties of a *S*-shaped multi-iron substituted arsenotungstate $[enH_2]_2[(\alpha\text{-}H_2As^{V}W_6O_{26})Fe_3(H_2O)(B\text{-}\alpha\text{-}H_4As^{V}W_9O_{34})]_2[Fe]_2\cdot 8H_2O$ (**1**).

* Corresponding authors. Fax: +86 378 3886876.
E-mail addresses: zhaojunwei@henu.edu.cn (J. Zhao), jyniu@henu.edu.cn (J. Niu).

0022-4596/$ - see front matter © 2011 Elsevier Inc. All rights reserved.
doi:10.1016/j.jssc.2011.08.016

2. Experimental

2.1. Materials and methods

The precursor $K_{14}[As^{III}_2W_{19}O_{67}(H_2O)]\cdot nH_2O$ was synthesized as previously described [10]. All reagents for synthesis were purchased from commercial sources and used without further purification. Elemental analyses (C, H and N) were performed on a Perkin-Elmer 240C elemental analyzer. Inductively coupled plasma (ICP) spectra were performed on a Perkin-Elmer Optima 2000 ICP-OES spectrometer. The IR spectrum was obtained from a solid sample palletized with KBr on Nicolet 170 SXFT-IR spectrometer in the range 400–4000 cm^{-1}. The UV spectrum was obtained with a U-4100 spectrometer at room temperature. The powder X-ray diffraction spectrum was performed on a Philips X'Pert-MPD instrument with Cu $K\alpha$ radiation ($\lambda=1.54056$ Å) at 293 K. Magnetic susceptibility measurements were carried out with a Quantum Design MPMS-XL-7 magnetometer in the temperature range of 1.8–300 K. The susceptibility data were corrected from the diamagnetic contributions as deduced using Pascal's constant tables.

2.2. Synthesis of $[enH_2]_2[(\alpha\text{-}H_2As^VW_6O_{26})Fe_3(H_2O)(B\text{-}\alpha\text{-}H_4As^VW_9O_{34})]_2[Fe]_2\cdot 8H_2O$ (**1**)

$K_{14}[As^{III}_2W_{19}O_{67}(H_2O)]\cdot nH_2O$ (0.534 g, *ca.* 0.101 mmol) and $Fe_2(SO_4)_3\cdot H_2O$ (0.212 g, *ca.* 0.530 mmol) were suspended in H_2O (10 mL), to which en (0.05 mL, 0.740 mmol) and H_3PO_4 (0.05 mL, 1 mol L^{-1}) were added under stirring. The resulting mixture was adjusted to $pH_i=6.0$ using NaOH (1.0 mol L^{-1}), stirred for 2.5 h, sealed in a Teflon-lined stainless steel autoclave (25 mL), kept at 130 °C for 5 days and then cooled to room temperature ($pH_f=5.6$). Brown prismatic crystals were filtered, washed with distilled water and dried in air. Yield: ≈51%. Elemental analysis calcd (%) for $C_4H_{52}N_4O_{130}Fe_8As_4W_{30}$: C, 0.57; H, 0.62; N, 0.66; Fe, 5.26; As, 3.53; W, 64.90. Found: C, 0.68; H, 0.75; N, 0.74; Fe, 5.19; As, 3.59; W, 64.84. IR (KBr pellet, ν/cm^{-1}): 3479(s), 3130(s), 3130(s), 2916(w), 1616(s), 1508(m), 1336(m), 1049(s), 1020(s), 953(s), 886 (s), 811(s), 735(s), 675(s), 510(m), 457(m).

Table 1
X-ray crystallographic data for **1**.

	1
Empirical formula	$C_4H_{52}N_4O_{130}Fe_8As_4W_{30}$
Formula weight	8498.48
Crystal system	Monoclinic
Space group	C_2/m
a (Å)	30.369(11)
b (Å)	21.530(10)
c (Å)	11.891(5)
β (deg.)	113.05
V (Å^3)Å	7154(5)
Z	2
D_c (g cm^{-3})	3.945
Absorption coefficient (mm^{-1})	25.809
T (K)	296(2)
Limiting indices	$-36\le h\le 23$ $-23\le k\le 25$ $-13\le l\le 14$
No. of reflections collected	17,387
No. of independent reflections	6290
Data/restrains/parameters	6290/100/415
Goodness-of-fit on F^2	1.053
Final R indices [$I>2\sigma(I)$]	$R_1=0.0970$ $wR_2=0.2098$
R indices (all data)	$R_1=0.1897$ $wR_2=0.2403$

[a] $R_1=\sum||F_o|-|F_c||/\sum|F_o|$.
[b] $wR_2=[\sum w(F_o^2-F_c^2)^2/\sum w(F_o^2)^2]^{1/2}$.
$w=1/[\sigma^2(F_o^2)+(xP)^2+yP]$, $P=(F_o^2+2F_c^2)/3$, where $x=0.0522$, $y=0.0000$ for **1**.

2.3. X-ray crystallography

Intensity data of **1** were collected at 296 K using a Bruker Apex II diffractometer equipped with a CCD bidimensional detector with the graphite-monochromated Mo $K\alpha$ radiation ($\lambda=0.71073$ Å). The absorption correction was based on multiple and symmetry-equivalent reflections in the data set using the SADABS program. Direct methods were used to solve the structure and to locate the heavy atoms using the SHELXTL-97 program package [16,17]. The remaining atoms were found from successive full-matrix least-squares refinements on F^2 and the Fourier syntheses. No hydrogen atoms associated with water molecules were located from the difference Fourier map. Hydrogen atoms attached to carbon and nitrogen atoms were geometrically placed. All hydrogen atoms were refined isotropically as a riding mode using the default SHELXTL parameters. Crystallographic data and structure refinement parameters for **1** are summarized in Table 1.

3. Results and discussion

3.1. Synthesis

1 was hydrothermally prepared by a mixture of the divacant precursor $As^{III}_2W_{19}$, $Fe_2(SO_4)_3\cdot xH_2O$, en and H_3PO_4 with the pH=6.0 adjusted by NaOH at 130 °C. To date, **1** can be not synthesized by the reaction of $Na_8[\alpha\text{-}HAsW_9O_{34}]\cdot 11H_2O$ with $Fe_2(SO_4)_3\cdot H_2O$. Furthermore, H_3PO_4 plays a very important role in the formation of **1**, when H_3PO_4 was removed away from the reaction system, **1** cannot be obtained. The specific role of H_3PO_4 was not well understood and intensive investigation is in progress. As usually observed, the formation of **1** is also highly dependent on the pH value. **1** was formed in the pH region of 5.5–6.0, however, as reported $(C_2N_2H_{10})_{11}[(B\text{-}\alpha\text{-}PW_9O_{34})_3(OH)_3)_4(PO_4)_4Fe]\cdot 38H_2O$ was obtained when the pH was in the range of 6.1–6.7 [18]. Additional two points should be noted in the formation of **1**: (a) The $As^{III}_2W_{19}$ precursors were degraded to the $[B\text{-}\alpha\text{-}AsW_9O_{34}]^{9-}$ and $[\alpha\text{-}As^VW_6O_{26}]^{11-}$ fragments (Fig. S1); (b) The As^{III} atom in the precursor was oxidized to the As^V atom in **1** under hydrothermal conditions, which is supported by the case that the As^{III} atom in $As^{III}_2W_{19}$ is three-coordinate and the As^V atom in **1** is four-coordinate and the result of bond valence sum (BVS) calculations of the As^V atom in **1** [19]. Such phenomenon that the As^{III} atom was oxidized to the As^V atom under hydrothermal conditions was previously encountered [20,21]. We expected that using 1,2-diaminopropane in place of en would lead to an isostructural species to **1**, however, we failed. Currently, we are investigating the influence of the transition metal and organic ligands on the structural construction of products in this system.

3.2. Structure description

The phase purity of **1** is supported by the agreement of the powder X-ray diffraction (PXRD) pattern of the bulk with the calculated pattern from the single-crystal structural analysis (Fig. 1). The intensity difference between experimental and simulated PXRD patterns is due to the variation in preferred orientation of the powder sample during collection of the experimental PXRD. **1** crystallizes in the monoclinic space group C_2/m and is a molecular complex composed of a *S*-shaped entity of $\{[(\alpha\text{-}H_2As^VW_6O_{26})Fe_3(H_2O)\ (B\text{-}\alpha\text{-}H_4As^V\ W_9O_{34})]_2[Fe]_2\}^{4-}$ with 9.1×26.1 Å in size (abbreviated as $Fe_8As_4W_{30}$), two discrete diprontonated $[enH_2]^{2+}$ cations and eight lattice water molecules

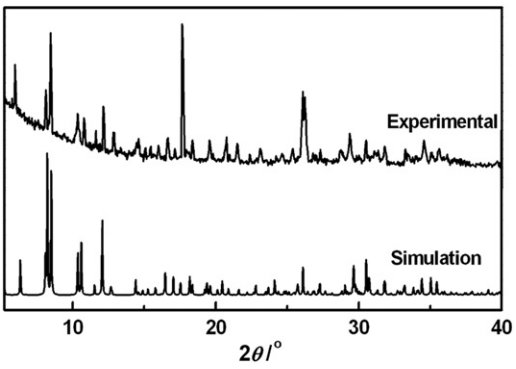

Fig. 1. PXRD pattern of **1** and its calculated pattern based on the single-crystal solution.

(Fig. 2a). The chemical valences of all the W, As and Fe atoms are completely determined by BVS calculations [19]. All the W atoms are +6, all the As atoms are +5 and all the Fe atoms are +3. Furthermore, two free en molecules should be diprontonated to form two $[enH_2]^{2+}$ cations. Actually, the phenomena that N-containing organic molecules are often prontonated under either acidic or basic conditions are very common in POM chemistry and coordination chemistry [18,22,23]. Considering the charge-neutrality principle, it is necessary to supplement twelve protons to the molecule of **1**. To determine the possible sites binding twelve protons, BVS calculations for all remaining oxygen atoms in the asymmetrical unit have been also performed (Table S1) [19]. The BVS value of O1W atom is 0.21, indicating that it is a coordination water molecule while the BVS values of O5, O6, O7 and O21 atoms are significantly lower than 2, indicating that these atoms are monoprotonateed. Because O5 and O7 atoms are situated in the special sites with the site occupancy of 0.5 and O6 and O21 atoms stand in the normal sites with the site occupancy of 1 (Fig. S2), the formula of **1** can be written as $[enH_2]_2[(\alpha\text{-}H_2As^{V}W_6O_{26})Fe_3(H_2O)(B\text{-}\alpha\text{-}H_4As^{V}W_9O_{34})]_2\ [Fe]_2\cdot 8H_2O$. The framework of $Fe_8As_4W_{30}$ can be viewed as a combination of two equivalently asymmetric sandwich-type subunits $[(\alpha\text{-}H_2As^{V}W_6O_{26})Fe_3(H_2O)(B\text{-}\alpha\text{-}H_4\ As^{V}W_9O_{34})]^{5-}$ (Fig. 2b) linked by a di-Fe^{III} cluster through eight μ_2-O and two μ_3-O bridges. The asymmetric sandwich-type subunit $(\alpha\text{-}H_2As^{V}W_6O_{26})Fe_3(H_2O)(B\text{-}\alpha\text{-}H_4As^{V}W_9O_{34})]^{5-}$ is established by a trivacant Keggin $[B\text{-}\alpha\text{-}As^{V}W_9O_{34}]^{9-}$ fragment and a hexavacant Keggin $[\alpha\text{-}As^{V}W_6O_{26}]^{11-}$ fragment linked by a nearly equilateral triangular tri-Fe^{III} cluster $[Fe_3(H_2O)]^{9+}$ via eight μ_2-O, three μ_3-O and one μ_4-O atoms. In the asymmetric sandwich-type subunit $[(\alpha\text{-}H_2As^{V}W_6\ O_{26})Fe_3(H_2O)(B\text{-}\alpha\text{-}H_4As^{V}W_9O_{34})]^{5-}$, three Fe^{III} cations reside in the FeO_6 octahedral geometry with Fe–O distances of 1.87(2)–2.36(4) Å and three edge-sharing FeO_6 octahedra generate the triangular tri-Fe^{III} cluster $[Fe_3(H_2O)]^{9+}$. Similar triangular edge-sharing tri-Fe^{III} cluster has been observed in the tetrameric phosphotungstate $(enH_2)_{3.5}H_{15}[\{Fe^{II}Fe^{III}_{12}(\mu_3\text{-}OH)_{12}(\mu_4\text{-}PO_4)_4\}(B\text{-}\alpha\text{-}PW_9O_{34})_4]\cdot 83H_2O$ [24]. As shown in Fig. 2c, two $[\alpha\text{-}As^{V}W_6O_{26}]^{11-}$ fragments on two asymmetric sandwich-type subunits are held together by two edge-sharing FeO_6 octahedra with Fe–O distances of 1.91(2)–2.18(2) Å. To our knowledge, the centric *S*-shaped $Fe_8As_4W_{30}$ represents the rare *S*-shaped POM consisting of two asymmetric sandwich-type subunits linked by a di-nuclear TM cluster though two *S*-shaped POMs $[\{(B\text{-}\beta\text{-}SiW_9O_{33}(OH))(\beta\text{-}SiW_8O_{29}(OH)_2)\ Co_3(H_2O)\}_2Co(H_2O)_2]^{20-}$ [25] and $[Mn(H_2O)_2\{Mn_3(H_2O)(B\text{-}\beta\text{-}GeW_9O_{33}(OH))(B\text{-}\beta\text{-}GeW_8O_{30}(OH))\}_2]^{22-}$ [26] built by two asymmetric sandwich-type subunits linked by a TM cation have been discovered by Mialane et al. and Kortz et al., respectively. An important feature of **1** is that it contains asymmetric sandwich -type POM units constituted by a trivacant Keggin $[B\text{-}\alpha\text{-}As^{V}W_9O_{34}]^{9-}$ and a hexavacant Keggin $[\alpha\text{-}As^{V}W_6O_{26}]^{11-}$ fragments. In a certain extent,

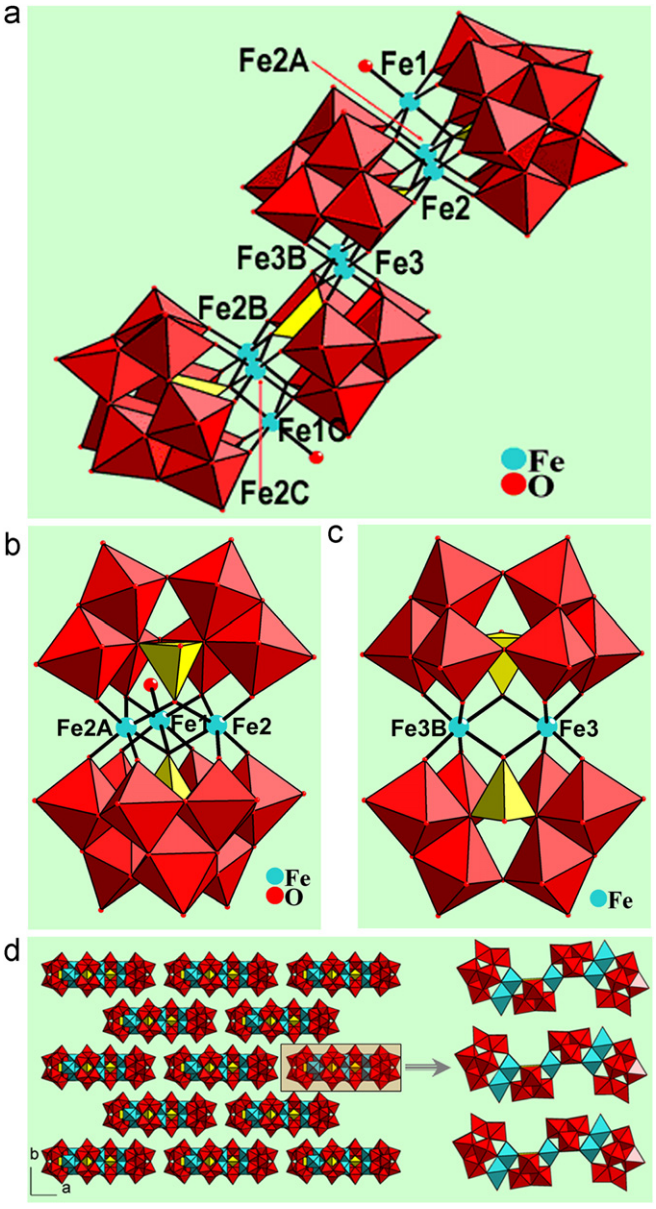

Fig. 2. (a) *S*-shaped framework of $Fe_8As_4W_{30}$ in **1** with selected numbering scheme. The atoms with "A, B, C" in their labels are symmetrically generated (A: $x, -y, z$; B: $-x, -y, 1-z$; C: $-x, y, 1-z$). (b) The asymmetrical sandwich-type $[(\alpha\text{-}H_2As^{V}W_6O_{26})Fe_3(H_2O)(B\text{-}\alpha\text{-}H_4As^{V}W_9O_{34})]^{5-}$ subunit. (c) The combination of two $[\alpha\text{-}AsW_6O_{26}]^{11-}$ and $[Fe_2]^{6+}$ subunits. (d) The packing arrangement of **1** viewed along the crystallographical *c* axis. Hydrogen atoms, free en molecules and lattice water molecules are omitted for clarity. WO_6 octahedra: red; AsO_4 tetrahedra: yellow; FeO_6 octahedra: aquamarine. (For interpretation of the references to color in this figure legend, the reader is referred to the web version of this article.)

the structure of **1** somewhat resembles that of the banana-shaped $[M_6As_3W_{24}O_{94}(H_2O)_2]^{17-}$ (M=Ni^{II}, Co^{II}, Mn^{II}, Zn^{II}) [27,28]. In addition, other asymmetric sandwich-type POMs encapsulating two nonequivalent Keggin fragments have been also reported in the past several years [25,26,29,30]. For example, in 2006, Wang et al. communicated a Ni_7-sandwiched silicotungstate $[Ni_7(OH)_4(H_2O)(CO_3)_2\ (HCO_3)(A\text{-}\alpha\text{-}SiW_9O_{34})(\beta\text{-}SiW_{10}O_{37})]^{10-}$ containing $[A\text{-}\alpha\text{-}SiW_9O_{34}]^{10-}$ and $[\beta\text{-}SiW_{10}O_{37}]^{10-}$ moieties [29]. In 2007, Lisnard et al. addressed an asymmetric sandwich-type POM $[Co_{1.5}(H_2O)_7)][(\gamma\text{-}SiW_{10}O_{36})(\beta\text{-}SiW_8O_{30}(OH))\ Co_4(OH)(H_2O)_7]^{7-}$ built by a $[\gamma\text{-}SiW_{10}O_{36}]^{8-}$ and a $[\beta\text{-}SiW_8O_{30}(OH)]^{9-}$ fragments connected by a mononuclear $\{CoO_4(H_2O)_2\}$ group and a $\{Co_3O_7(OH)\ (H_2O)_5\}$ cluster [25]. In 2007 and 2009, Kortz's group discovered the asymmetric

sandwich-type $[K(H_2O)(\beta\text{-}Fe_2GeW_{10}O_{37}(OH))(\gamma\text{-}GeW_{10};O_{36})]^{12-}$ [30] and $[Cu_3(H_2O)(B\text{-}\beta\text{-}GeW_9O_{33}(OH))(B\text{-}\beta\text{-}GeW_8O_{30}(OH))]^{12-}$ [26]. In **1**, neighboring *S*-shaped $Fe_8As_4W_{30}$ entities are oriented parallel to each other, resulting in layers in the *ab* plane that are offset to each other with the manner of –ABAB– (Fig. 2d).

3.3. IR and UV spectra

The IR spectrum of **1** exhibits four characteristic vibration absorption bands derived from the lacunary Keggin POM fragments at 953, 886, 735 and 675 cm^{-1}, which are assigned to the $\nu(W\text{–}O_t)$, $\nu(As\text{–}O_a)$, $\nu(W\text{–}O_b)$ and $\nu(W\text{–}O_c)$ stretching vibration patterns, respectively (Fig. S3) [31]. The stretching bands of $–NH_2$ and $–CH_2$ groups are observed at 3130 and 2916 cm^{-1}, respectively, and the bending vibration bands of $–NH_2$ and $–CH_2$ groups also appear at 1616 and 1501 cm^{-1}, respectively, which suggests the presence of en in **1**. The UV spectrum of **1** has been performed in an aqueous solution in the range of 190–400 nm (Fig. S4) and reveals one broad absorption band at 261 nm, which is ascribed to the $p\pi\text{–}d\pi$ charge transfer transitions of the $O_{b(c)}\rightarrow W$ bonds [32]. However, the higher energy absorption band attributed to the $p\pi\text{–}d\pi$ charge-transfer transitions of the $O_t\rightarrow W$ bonds is blue-shifted to the near UV region that is lower than 190 nm, which may be related to the interactions between free $[enH_2]^{2+}$ cations and POM matrixes. Such a phenomenon has been already encountered in our previous studies [33,34].

3.4. Magnetic properties

The magnetic behavior of **1** was investigated between 1.8 and 300 K (Fig. 3a). The χ_M slowly increases from 0.09 emu mol^{-1} at 300 K to 0.46 emu mol^{-1} at 20 K and then exponentially to the maximum of 2.19 emu mol^{-1} at 1.8 K (Fig. S5). At 300 K, the $\chi_M T$ value of 28.27 emu K mol^{-1} is slightly lower than the calculated $\chi_M T$ value of 35.00 emu K mol^{-1} for eight noninteracting high-spin Fe^{III} ($S=5/2$) centers (assuming $g=2.00$), indicating weak antiferromagnetic interactions. This is also shown by the continuous decrease of the $\chi_M T$ value to 3.95 emu K mol^{-1} at 1.8 K upon sample cooling. Moreover, the magnetic susceptibility data between 55 and 300 K obey the Curie–Weiss law, affording $C=35.53$ emu K mol^{-1} and $\theta=-79.86$ K (Fig. S6), which consolidates the presence of the antiferromagnetic coupling within Fe^{III} centers.

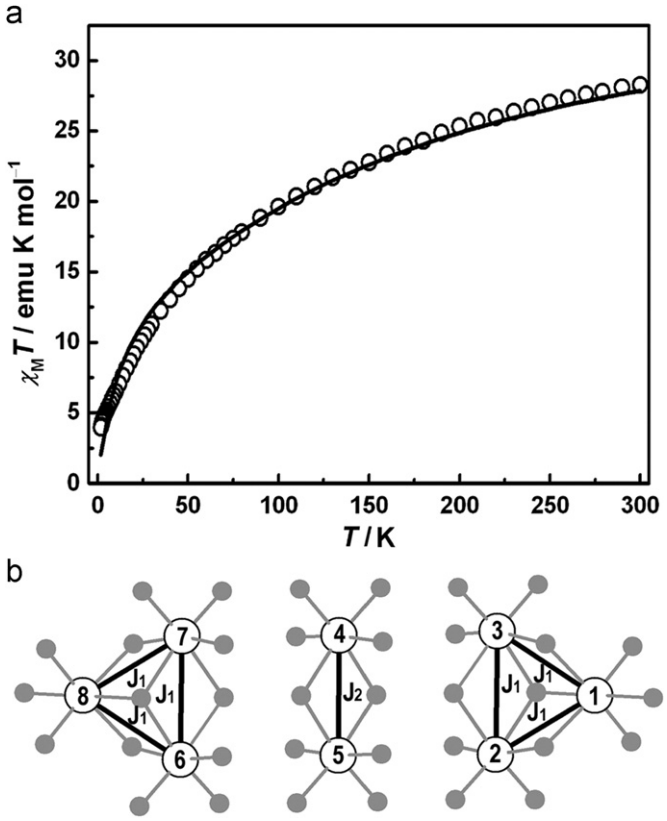

Fig. 3. (a) Plot of $\chi_M T$ versus T for **1** between 1.8 and 300 K. The solid line was generated from the best fit parameters given in the text. (b) The schematic magnetic exchange model in **1** showing the two main exchange interactions.

In order to quantitatively analyze the magnetic coupling interactions within Fe^{III} centers, we examined the structural parameters of **1**. As shown in Fig. 2a, the molecule of **1** consists of two tri-Fe^{III} clusters and one di-Fe^{III} cluster, which are well isolated by nonmagnetic $[B\text{-}\alpha\text{-}AsW_9O_{34}]^{9-}$ and $[\alpha\text{-}AsW_6O_{26}]^{11-}$ fragments. This situation offers us a good opportunity for probing the magnitude of magnetic exchange interactions. The magnetic exchange interactions between two tri-Fe^{III} clusters and one di-Fe^{III} cluster can be negligible. Thus, the magnetic behavior of **1** can be viewed as the addition of the magnetic behaviors of two tri-Fe^{III} clusters and one di-Fe^{III} cluster. Because the exchange interactions within two tri-Fe^{III} clusters and one di-Fe^{III} cluster are mediated through the oxo-bridges, it is important to examine the distances of $Fe\cdots Fe$ and the angles of $\angle$Fe–O–Fe. As the molecule of **1** possesses the C_2 symmetry, two tri-Fe^{III} clusters are equivalent. In the tri-Fe^{III} cluster, the Fe–Fe distances vary in 3.29–3.47 Å and the angles of $\angle$Fe–O–Fe range from 93.6 to 106.7°. In the di-Fe^{III} cluster, the $Fe\cdots Fe$ distance is 3.36 Å and the angle of $\angle$Fe–O–Fe is 100.7°. According to the classical correlation between the $\angle$Fe–O–Fe angles and the magnetic coupling constants within polynuclear iron compounds, when the $\angle$Fe–O–Fe angles are larger than 90°, the compound reveals the antiferromagnetic couplings [35]. Meanwhile, using the formulation $J=A(B+C\cos\varphi+\cos^2\varphi)\exp(Dr)$ (φ=Fe–O–Fe angle; r=Fe–O distance) based on the angular overlap model can also confirm this conclusion [36]. In **1**, all $\angle$Fe–O–Fe angles range from 93.6 to 106.7°, as a result, the antiferromagnetic couplings are also predicted in **1**. Accordingly, we have fitted the magnetic data to a simple isotropic model regardless of the negligible magnetic exchange interactions between two tri-Fe^{III} clusters and one di-Fe^{III} cluster because they are excellently separated by a nonmagnetic $[\alpha\text{-}AsW_6O_{26}]^{11-}$ fragment. The magnetic exchange model of two tri-Fe^{III} clusters and one di-Fe^{III} cluster in **1** is shown in Fig. 3b, the vertices with numbers 1, 2, 3, 4, 5, 6, 7 and 8 symbolize Fe1, Fe2, Fe2A, Fe3B, Fe3, Fe2C, Fe2B and Fe1C, respectively (Fig. 2a). The magnetic exchange constants of $Fe1\cdots Fe2$, $Fe1\cdots Fe2A$, $Fe2\cdots Fe2A$, $Fe2C\cdots Fe2B$, $Fe2C\cdots Fe1C$ and $Fe1C\cdots Fe2B$ are defined as J_1 while the magnetic exchange constant of $Fe3\cdots Fe3B$ is defined as J_2. Thus, the isostropic spin Hamiltonian for two tri-Fe^{III} clusters and one di-Fe^{III} cluster in **1** with $S_1=S_2=S_3=S_4=S_5=S_6=S_7=S_8=5/2$ can be described as:

$$H=-2J_1(S_1S_2+S_1S_3+S_2S_3+S_6S_7+S_6S_8+S_7S_8)-2J_2S_3S_4$$

The expression of the molar susceptibility can be obtained as follows by addition of the expressions of the molar susceptibilities of two tri-Fe^{III} clusters [37] and one di-Fe^{III} cluster [38] derived from for spin pairs coupled through the isotropic exchange interactions:

$$\chi_M=2\frac{N\beta^2g^2}{4kT}\left(\frac{\begin{array}{l}1+20\exp(3x)+105\exp(8x)+210\exp(15x)\\+330\exp(24x)+429\exp(35x)\\+455\exp(48x)+340\exp(63x)\end{array}}{\begin{array}{l}1+4\exp(3x)+9\exp(8x)+10\exp(15x)\\+10\exp(24x)+9\exp(35x)+7\exp(48x)\\+4\exp(63x)\end{array}}\right)$$

$$+\frac{N\beta^2 g^2}{kT}\left(\frac{2\exp(2y)+10\exp(6y)+28\exp(12y)+60\exp(20y)+110\exp(30y)}{1+3\exp(2y)+5\exp(6y)+7\exp(12y)+9\exp(20y)+11\exp(30y)}\right)$$

where $x=J_1/kT$, $y=J_2/kT$. The best-fitting set of parameters are $J_1=-7.07\ cm^{-1}$, $J_2=-0.45\ cm^{-1}$, $g=2.05$ and $R=[\sum\chi_{obsd}T-\chi_{calcd}T)^2/\sum\chi_{obsd}T)^2]=6.0\times10^{-3}$. The negative J_1 and J_2 values further confirm the occurrence of the relatively weak antiferromagnetic exchange interactions within tri-Fe^{III} clusters and di-Fe^{III} cluster via the oxygen bridges. In the previously reported Fe^{III}-containing complexes, there are four possible magnetic exchange pathways coming from t_{2g}–t_{2g}, e_g–e_g and t_{2g}–e_g interactions [37,38]. The antiferromagnetic interactions can occur when two interacting orbitals (t_{2g}–t_{2g} or e_g–e_g) contain an unpaired electron (SOMO–SOMO interactions), while the ferromagnetic interactions can occur when the orbitals are orthogonal (t_{2g}–e_g interactions) or one orbital containing an unpaired electron interacts with an empty orbital (SOMO–LUMO interactions via the e_g–e_g pathway). For the high-spin Fe^{III} center with the octahedral geometry, SOMO–SOMO interactions via the t_{2g}–t_{2g} and e_g–e_g pathway are dominant [39,40]. Hence, the antiferromagnetic behavior of **1** is readily expected. Furthermore, the antiferromagnetic couplings of the Fe^{III}–O cluster substituted polyoxotungstates are very common in POM chemistry [13]. For example, in 2005, Godin et al. [41] reported two novel high-nuclearity Fe^{III} substituted $\{P_2W_{12}\}$-based aggregates $[H_4P_2W_{12}Fe_9O_{56}(OAc)_7]^{6-}$ and $[H_{55}P_8W_{49}Fe_{27}O_{248}]^{26-}$, which indicate the strong intramolecular antiferromagnetic coupling between the Fe^{III} centers. In the same year, an antiferromagnetic trigonal prismatic hexa-Fe^{III} substituted tungstogermanate $[Fe_6(OH)_3(A\text{-}\alpha\text{-}GeW_9O_{34}(OH)_3)_2]^{11-}$ was also discovered by Kortz et al. [42]. In 2008, Dolbecq's group addressed a square POM built up of four disubstituted $[\alpha\text{-}PW_{10}Fe^{III}_2O_{39}]^{7-}$ anions, which exhibits the occurrence of antiferromagnetic interactions [18].

4. Conclusions

In summary, a *S*-shaped multi-iron substituted arsenotungstate containing asymmetric sandwich-type subunits linked by a symmetric di-TM cluster has been hydrothermally synthesized. An important feature of **1** is that it contains asymmetric sandwich-type POM units constituted by a trivacant Keggin $[B\text{-}\alpha\text{-}As^VW_9O_{34}]^{9-}$ and a hexavacant Keggin $[\alpha\text{-}As^VW_6O_{26}]^{11-}$ fragments. Its magnetic properties have also been quantitatively investigated. The successful synthesis of **1** illustrates that we can design and prepare novel TM-subsituted aggregates by means of the structural diversity and facile polymerization of the lacunary $As^{III}_2W_{19}$ precursor. In the following work, we will deeply exploit this system by changing different TM or Ln cations.

Supplementary data

CCDC 736213 contains the supplementary crystallographic data for this paper for **1**. These data can be obtained free of charge from the Cambridge Crystallographic Data Centre via www.ccdc.cam.ac.uk/data_request/cif. Supplementary data associated with this article can be found in the online version at doi:10.1016/j.jssc.2011.03.030.

Acknowledgments

We are thankful for financial support from the Natural Science Foundation of China (21101055, 21071043), China Postdoctoral Science Foundation funded project (20100470996), the Natural Science Foundation of Henan Province (Nos. 092300410119 and 102300410093), the Natural Science Foundation of Henan University (No. 2008YBZR010), the Postdoctoral Science Foundation of Henan University (No. BH2010003) and the Foundation of Education Department of Henan Province (Nos. 2009A150003 and 2010B150006).

Appendix A. Supplementary material

Supplementary data associated with this article can be found in the online version at doi:10.1016/j.jssc.2011.08.016.

References

[1] J.-D. Compain, P. Mialane, A. Dolbecq, I.M. Mbomekallé, J. Marrot, F. Sécheresse, E. Rivière, G. Rogez, W. Wernsdorfer, Angew. Chem. Int. Ed. 48 (2009) 3077–3081.
[2] C.Y. Duan, M.L. Wei, D. Guo, C. He, Q.J. Meng, J. Am. Chem. Soc. 132 (2010) 3321–3330.
[3] C.Y. Sun, S.X. Liu, D.D. Liang, K.Z. Shao, Y.H. Ren, Z.M. Su, J. Am. Chem. Soc. 131 (2009) 1883–1888.
[4] Z.M. Zhang, S. Yao, Y.G. Li, Y.H. Wang, Y.F. Qi, E.B. Wang, Chem. Commun. (2008) 1650–1652.
[5] S.T. Zheng, J. Zhang, J.M. Clemente-Juan, D.Q. Yuan, G.Y. Yang, Angew. Chem. Int. Ed. 48 (2009) 7176–7179.
[6] J.W. Zhao, C.M. Wang, J. Zhang, S.T. Zheng, G.Y. Yang, Chem. Eur. J. 14 (2008) 9223–9239.
[7] D.J. Guo, S.J. Fu, W. Tan, Z.D. Dai, J. Mater. Chem. 20 (2010) 10159–10168.
[8] C. Tourné, A. Revel, G. Tourné, M. Vendrell, C.R. Hebd, Seances Acad. Sci. Ser. C 277 (1973) 643–645.
[9] C. Tourné, G. Tourné, C.R. Acad. Sci., Ser. C 281 (1975) 933–936.
[10] U. Kortz, M.G. Savelieff, B.S. Bassil, M.H. Dickman, Angew. Chem. Int. Ed. 40 (2001) 3384–3386.
[11] F. Hussain, M. Reicke, U. Kortz, Eur. J. Inorg. Chem. (2004) 2733–2738.
[12] F. Hussain, B.S. Bassil, U. Kortz, O.A. Kholdeeva, M.N. Timofeeva, P. de Oliveira, B. Keita, L. Nadjo, Chem. Eur. J. 13 (2007) 4733–4742.
[13] S. Chang, Y.F. Qi, E.B. Wang, Y.G. Li, H. Jin, J. Cluster Sci. 18 (2007) 781–796.
[14] S. Chang, Z.M. Zhang, Y.G. Li, S. Yao, E.B. Wang, Aust. J. Chem. 63 (2010) 680–686.
[15] F. Hussain, F. Conrad, G.R. Patzke, Angew. Chem. Int. Ed. 48 (2009) 9088–9091.
[16] G.M. Sheldrick, SHELXS97, Program for Crystal Structure Solution, University of Göttingen, Göttingen, Germany, 1997.
[17] G.M. Sheldrick, SHELXL97, Program for Crystal Structure Refinement, University of Göttingen, Göttingen, Germany, 1997.
[18] C. Pichon, A. Dolbecq, P. Mialane, J. Marrot, E. Rivière, F. Sécheresse, Dalton Trans. (2008) 71–76.
[19] I.D. Brown, Altermatt, Acta Cryst. B41 (1985) 244–247.
[20] E.G. Fidalgo, A. Neels, H. Stoeckli-Evans, G. Süss-Fink, Polyhedron 21 (2002) 1921–1928.
[21] J.W. Zhao, C.H. Liu, L.J. Chen, P.T. Ma, J.P. Wang, Chinese J. Struct. Chem. 29 (2010) 599–607.
[22] M. Hölscher, U. Englert, B. Zibrowius, W.F. Hölderich, Angew. Chem. Int. Ed. 33 (1994) 2491–2493.
[23] C. Pichon, A. Dolbecq, P. Mialane, J. Marrot, E. Rivière, M. Goral, M. Zynek, T. McCormac, S.A. Borshch, E. Zueva, F. Sécheresse, Chem. Eur. J. 14 (2008) 3189–3199.
[24] J.W. Zhao, J. Zhang, S.T. Zheng, G.Y. Yang, Inorg. Chem. 46 (2007) 10944–10946.
[25] L. Lisnard, P. Mialane, A. Dolbecq, J. Marrot, J.M. Clemente-Juan, E. Coronado, B. Keita, P. de Oliveira, L. Nadjo, F. Sécheresse, Chem. Eur. J. 13 (2007) 3525–3536.
[26] N.H. Nsouli, A.H. Ismail, I.S. Helgadottir, M.H. Dickman, J.M. Clemente-Juan, U. Kortz, Inorg. Chem. 48 (2009) 5884–5890.
[27] I.M. Mbomekalle, B. Keita, M. Nierlich, U. Kortz, P. Berthet, L. Nadjo, Inorg. Chem. 42 (2003) 5143–5152.
[28] K. Fukaya, T. Yamase, Bull. Chem. Soc. Jpn. 80 (2007) 178–182.
[29] Z. Zhang, Y. Li, E. Wang, C. Qin, H. An, Inorg. Chem. 45 (2006) 4313–4315.
[30] N.H. Nsouli, S.S. Mal, M.H. Dickman, U. Kortz, B. Keita, L. Nadjo, J.M. Clemente-Juan, Inorg. Chem. 46 (2007) 8763–8870.
[31] L.J. Chen, J.W. Zhao, P.T. Ma, Q.X. Han, J.P. Wang, J.Y. Niu, Inorg. Chem. Commun. 13 (2010) 50–53.
[32] L.H. Bi, R.D. Huang, J. Peng, E.B. Wang, Y.H. Wang, C.W. Hu, J. Chem. Soc. Dalton Trans. (2001) 121–129.
[33] J.W. Zhao, D.Y. Shi, L.J. Chen, P.T. Ma, J.P. Wang, J.Y. Niu, CrystEngComm 13 (2011) 3462–3469.
[34] J.Y. Niu, K.H. Wang, H.N. Chen, J.W. Zhao, P.T. Ma, J.P. Wang, M.L. Li, Y. Bai, D.B. Dang, Cryst. Growth Des. 9 (2009) 4362–4372.

[35] C. Cañana-Vilalta, T.A. O'Brien, E.K. Brechin, M. Pink, E.R. Davidson, G. Christou, Inorg. Chem. 43 (2004) 5505–5521.
[36] H. Weihe, H.U. Güdel, J. Am. Chem. Soc. 119 (1997) 6539–6543.
[37] R.W. Adams, C.G. Barraclough, R.L. Martin, G. Winter, Inorg. Chem. 5 (1966) 346.
[38] A. Hazell, K.B. Jensen, C.J. McKenzie, H. Toftlund, Inorg. Chem. 33 (1994) 3127–3134.
[39] S. Triki, F. Bérézovsky, J.S. Pala, E. Coronado, C.J. Gómez-García, J.M. Clemente, A. Riou, P. Molinié, Inorg. Chem. 39 (2000) 3771–3776.
[40] H.P. Jia, W. Li, Z.F. Ju, J. Zhang, J. Mol. Struct. 833 (2007) 49–52.
[41] B. Godin, Y.G. Chen, J. Vaissermann, L. Ruhlmann, M. Verdaguer, P. Gouzerh, Angew. Chem. Int. Ed. 44 (2005) 3072–3075.
[42] L.H. Bi, U. Kortz, S. Nellutla, A.C. Stowe, J. van Tol, N.S. Dalal, B. Keita, L. Nadjo, Inorg. Chem. 44 (2005) 896–903.